J. Fluid Mech. (2007), *vol.* 584, *pp.* 433–453.
doi:10.1017/S0022112007006702 Printed in the United Kingdom

Experiments on gravity currents propagating down slopes. Part 1. The release of a fixed volume of heavy fluid from an enclosed lock into an open channel

T. MAXWORTHY[1,2] AND R. I. NOKES[1]

[1]Department of Civil Engineering, University of Canterbury, Christchurch, New Zealand

[2]Department of Aerospace and Mechanical Engineering, University of Southern California, Los Angeles, CA, 98009-1191, USA
maxworth@usc.edu

(Received 25 May 2006 and in revised form 27 March 2007)

Gravity currents formed by the release of heavy fluid from an enclosed lock on a sloping open channel were investigated experimentally. The experiments were conducted in a channel that had a running length of 13 lock depths, and could be inclined to a maximum angle of 17°. The release of heavy dyed salt solution from a lock with an aspect ratio (height to length) of 0.5, was examined using video images to determine the front velocity, and a particle-tracking technique was used to measure the two-dimensional velocity field in a vertical slice through the centre of the evolving current. The gravity current head velocity increased with time and downstream distance to a maximum at approximately 10 lock depths from the front of the lock. Flow visualization and the velocity measurements have shown that during the acceleration phase the head was being fed by a following current that increased its buoyancy as it propagated downstream. A modified version of the theory of P. Beghin, E. J. Hopfinger and R. E. Britter (*J. Fluid Mech.* vol. 107, 1981, p. 407) in which the measured increase in buoyancy was used, instead of the original assumption of constant buoyancy, gave results that agreed closely with the experimental velocity versus time histories.

1. Introduction

The environmentally important problem of gravity current motion over a horizontal surface has received much attention and Simpson (1997) reviews a wide range of applications and laboratory studies.

There has been much less work on the problem of the motion of gravity currents down slopes. Britter & Linden (1980) considered the case of a constant flow rate of heavy fluid down slopes at angles to the horizontal (θ) from 5° to 90°. The theory they presented made use of experiments by Ellison & Turner (1959) on turbulent entrainment into a steady constant flow-rate density current flowing down a slope and used it to estimate the flow rate into the head of the current and hence its velocity. Although this work has some relevance to our work, which is, in essence, an unsteady version of their problem, it is the experiments by the LEGI group at the IMG of the University of Grenoble and collaborators that is used in what follows (see Tochon-Danguey 1977; Hopfinger & Tochon-Danguey 1977; Beghin, Hopfinger & Britter 1981; Laval *et al.* 1988; Rastello & Hopfinger 2004; Etienne, Hopfinger & Saramito 2006).

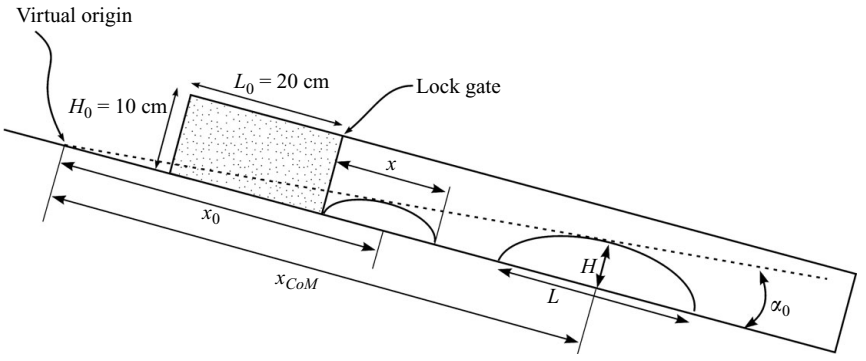

FIGURE 1. Definition sketch for the quantities used in the theory and elsewhere. H and L are the head height and length; x is the distance the front of the head has moved from the lock exit; x_0 is the distance from the virtual origin (VO) to the centre of mass (CoM) at the start of the motion, assumed to be at $x = 20$ cm so that the CoM was about 10 cm from the lock gate; x_{CoM} is the distance from the VO to the CoM). x and x_{CoM} have been made dimensionless using either x_0 and/or H_0 in what follows. θ is the channel slope and α_0 the spreading angle of the head, the value of which depends on the range of x over which it is measured, as discussed in the text. Note that in most cases, the head of the starting current contained only a fraction of the total, initial charge, $L_0 H_0$. Also, as implied by the title, the lock was closed, i.e. had a top cover, while the channel itself was open and did not have a cover.

Kersey & Hsu (1976), and Luthi (1980) investigated the problem of a gravity current on a slope, generated by the release of a finite volume of negatively buoyant material. However, the first study that considered a significant range of slope angles and combined an experimental study with a predictive mathematical model was Beghin *et al.* (1981). Their model, based on the bulk properties of the gravity current head, has formed the basis for many of the subsequent models found in the literature, including that presented in § 4, so a brief outline of this model is given below.

Consider the initial conditions shown in figure 1. A finite volume of dense fluid, of density ρ, is confined within a lock of length L_0 and depth H_0, on a sloping channel that is at an angle of θ to the horizontal, and is filled with fluid of density ρ_A. At $t = 0$, the gate at the front of the lock is removed and the dense fluid accelerates downslope. Observations show the rapid establishment of a bulbous head that grows as it propagates down the channel, followed by a thin tail that drains the lock fluid that remains after the head of the current exits the lock. Figure 2 illustrates the flow development for the case of a 17° slope.

Beghin *et al.* (1981) proposed a model for the flow based on a bulk parameterization of the motion of the current head. They assumed that the head contained a fixed amount of buoyancy, determined by the initial conditions in the lock, and that it entrained ambient fluid as it propagated down the channel. The head was assumed to have a self-similar form throughout its motion. The model is based on statements of conservation of mass and momentum for the head of the current and is an extension of the theory developed for thermals by Escudier & Maxworthy (1973). The rate of change of the total linear momentum of the head (or thermal), based on the Boussinesq assumption, i.e. $(\rho - \rho_A)/\rho_A \ll 1$, is

$$\frac{\mathrm{d}(\rho_A(1 + k_v)S_1 HLU)}{\mathrm{d}t} = B \sin\theta, \tag{1}$$

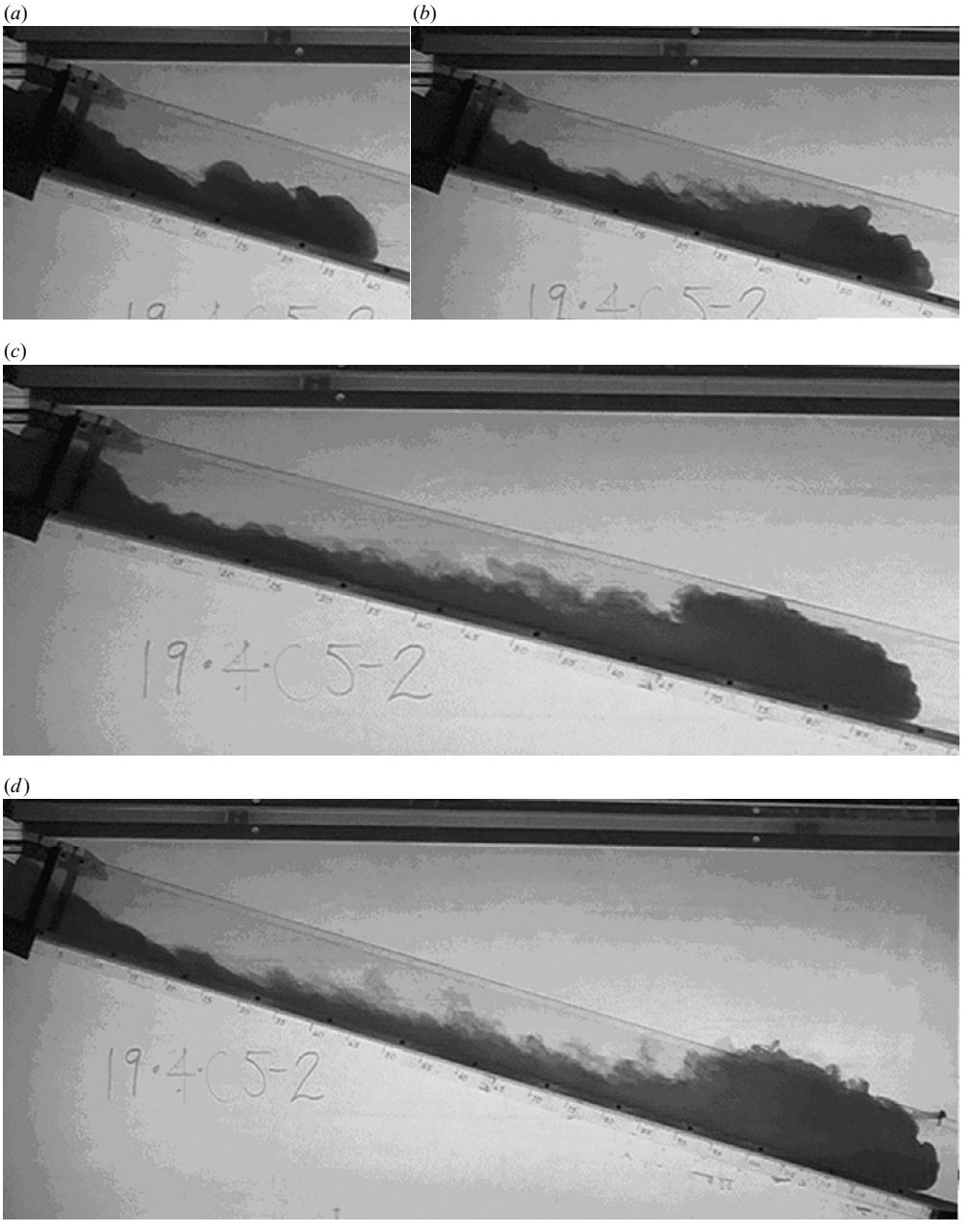

FIGURE 2. A heavy salt solution propagating down a slope at $\theta = 17^0$ to the horizontal. Time runs from the top left to the bottom. The times at which the images were taken after the gate was removed were (*a*) 11.9 s (*b*) 16.2 s (*c*) 24.3 s (*d*) 32.3 s. The spacing between the ruler markings along the base of the sloping channel is 5 cm. The reduced gravity was $g' = 2.55\,\mathrm{cm\,s^{-2}}$. Note the thick following layer which is feeding buoyancy into the head over most of the run.

where B is the total buoyancy in the head, defined to be

$$B = g(\rho - \rho_A)S_1 HL, \tag{2}$$

H and L are the height and length of the head, respectively, S_1 is a shape factor,

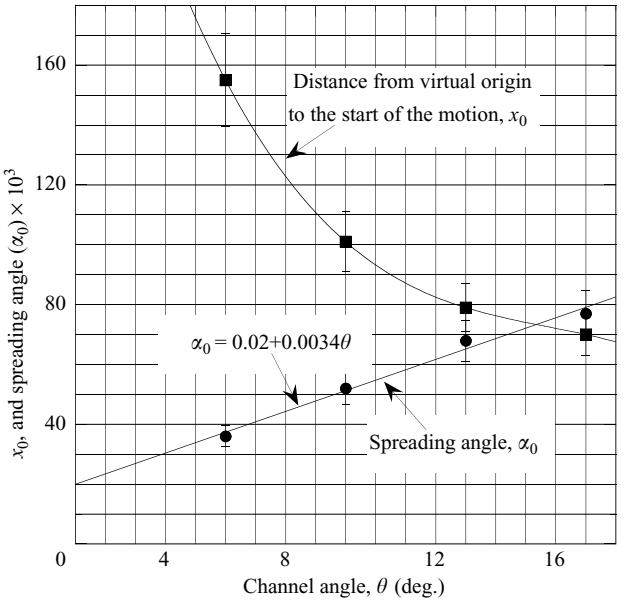

FIGURE 3. Spreading angle α_0 and distance from virtual origin to the start of the motion, x_0, measured in cm. Data points represent averages over all experiments at a given angle, and the error bars indicate the spread between the maximum and minimum values for experiments at each angle.

defined by $S_1 =$ cross-sectional area$/HL$, U is the centre of mass velocity, g is the acceleration due to gravity and k_v is an added mass coefficient. Beghin *et al.* (1981) assumed that the head takes the form of an elliptic cylinder for which $k_v = 2k$ where k is the aspect ratio of the cylinder given by H/L. Note that, as in Escudier & Maxworthy (1973) and Rastello & Hopfinger (2004), equation (1) can be easily modified to consider non-Boussinesq effects by writing the first two terms in the large bracket as $(\rho + k_v \rho_A)$.

In order to solve the momentum equation for the centre of mass velocity, the growth of the length and height of the head are required. Beghin *et al.* (1981) derive this behaviour from a conservation of mass equation which is based on entrainment of ambient fluid through the head boundary. Thus,

$$\frac{\mathrm{d}(S_1 HL)}{\mathrm{d}t} = S_2 (HL)^{1/2} \alpha(\theta) U, \tag{3}$$

where S_2 is a second shape factor given by $S_2 = (\pi/2^{3/2})(4k^2+1)^{1/2}/k^{1/2}$, i.e. the circumference$/(\mathrm{HL})^{1/2}$ and α is an entrainment coefficient that may be slope dependent. Equation (3) yields self-similar solutions for both H and L that grow linearly with x, measured from a virtual origin x_0 (see figure 1), and these solutions agree with both their, and our, experimental observations. Note that the spreading angle α_0, shown in figure 1 and plotted in figure 3, is related to α by

$$\alpha_0 = S_2 k^{1/2} \alpha / 2 S_1. \tag{4}$$

Finally, an analytic solution to (1) can be found using the derived expressions for H and L. The resulting solution in non-dimensional form is:

$$Fr^2 = \frac{Fr_0^2}{X_B^4} + C\left(\frac{1}{X_B} - \frac{1}{X_B^4}\right), \tag{5}$$

where $Fr = U/\sqrt{g'H_0}$, $Fr_0 = U_0/\sqrt{g'H_0}$, $g' = g(\rho - \rho_A)/\rho_A$ is the reduced gravity based on the original density of the lock fluid, and $X_B = x_{CoM}/x_0$ (see figure 1) is the dimensionless distance of the centre of mass measured from the virtual origin. U_0 is the initial velocity of the centre of mass, typically defined at $X_B = 1$. The constant C is defined to be:

$$C = \frac{8S_1 B \sin\theta}{3\rho_A(1 + k_v)\alpha^2 S_2^2 x_0 g' H_0}. \tag{6}$$

When the current starts from rest, the model predicts that, after an initial acceleration phase, the centre of mass of the current head decelerates once it has reached the downstream position

$$X_B = 4^{1/3}. \tag{7}$$

In this latter phase, the velocity of the centre of mass decreases with the square root of the distance from the virtual origin. If the current starts with a positive speed, then the distance at which the deceleration phase begins is less than that given in (7).

Our results, presented in § 2, demonstrate an acceleration phase that extends well beyond the downstream distance given in (7). This apparent discrepancy can be explained by the observation that the head of the current is being fed by the following flow for a considerable distance from the release point. This feature of the flow is explored quantitatively in § 3 and the experimental results of this section are used to modify the theory of Beghin *et al.* (1981) in § 4. The result is a successful description of the present experiments and a refined interpretation of the results of Beghin *et al.* (1981).

Others have built their models of related flows on that of Beghin *et al.* (1981). Webber, Jones & Martin (1993) developed a model for a three-dimensional gas cloud propagating downslope. Their model did not include entrainment and required the specification of a front condition, as did the model of Tickle (1996) who also considered a three-dimensional cloud, but now with entrainment incorporated. Ross, Linden & Dalziel (2002) analysed the release of a dense 'blob' on a slope. They assumed the shape of the blob took the form of a wedge, of assumed geometry, and solved a momentum equation, similar to that of Beghin *et al.* (1981), which included the effects of buoyancy and drag. They also assumed that the wedge entrained ambient fluid. Alavian (1986) also considered three-dimensional sources.

Rastello & Hopfinger (2004), who considered the motion of snow-powder avalanches also included bottom friction, entrainment of particles from an erodible bed and non-Boussinesq effects. The effect of the entrainment from the bed is to provide a varying buoyancy force. Their formulation was anticipated by Escudier & Maxworthy (1973) who generated an essentially identical non-Boussinesq theory for spherical thermals.

A numerical study of the lock-exchange problem in an enclosed channel on a slope, where the lock region and test region have equal lengths and the top of the channel is closed, is described in Birman *et al.* (2007). In this case, the two-dimensional numerical simulations give a head velocity that rises rapidly to a constant velocity that lasts for about ten lock lengths and then enters an unsteady phase. In agreement with what follows, they also found a feeding current from the main volume of the lock contents

that maintained a high head velocity. Other recent numerical simulations by Etienne *et al.* (2006) considered both Boussinesq and non-Boussinesq clouds where virtually all the initial discharge enters the head at the beginning of the motion and they give results that are close to the experiments of Beghin *et al.* (1981).

2. Dye experiments

2.1. *Apparatus and experimental procedures*

An idealized sketch of the channel used in these experiments is provided in figure 1. This figure also includes the important length scales used in the theory of § 4. The channel has a total length of 150 cm, an internal width of 12.5 cm and a height of $H_0 = 10$ cm. One end, 20 cm long (L_0), was completely enclosed by a top plastic sheet and a sliding lock gate facing the main 130 cm long channel. Two valved access-holes were drilled and tapped into the upper end of the top plate, one to allow filling with 2500 cm^3 of the test fluid and the other the escape of trapped air. Both were closed after the lock was charged. This open channel was placed in a blocked-off section, 250 cm long, 65 cm high $\times$ 15 cm wide, of an existing flume so that it was exposed to the total height of the water column to the free surface. In contrast to many examples in the literature it was not a closed constant-depth channel. Within this restricted geometry, it was only possible to raise the channel to a maximum 17° angle to the horizontal. In all experiments, this section was filled with fresh water to a depth of 10 cm above the upper edge of the lock.

These experiments involved the release of a fixed volume of salty fluid of known density, the latter being measured using an Anton Paar Model 602C density meter that gave densities at 20°C, accurate to five decimal places. The use of small density differences required the temperature of both the released and receiving water to be measured to an accuracy of 0.1 K and corrections made for any differences in density owing to temperature. All of the experiments were recorded with two video cameras.

2.2. *Results*

Video images from a typical experiment, with a slope of 17°, are shown in figure 2. The flow has a high $Re = g'^{1/2} H_0^{3/2}/\nu$ and is very turbulent, ν is the kinematic viscosity. A bulbous, approximately semi-elliptical head is seen to grow with downstream distance, and is followed by a tail that links the current head to the fluid remaining within the lock. This tail thins with time. Experiments run at smaller angles had the same basic characteristics except that the growth rate of the head became progressively smaller as the angle decreased.

For each experiment, the geometric properties of the head were measured, namely, the aspect ratio of the current head, $k = H/L$, the spreading angle of the head growth, α_0, and the location of the virtual origin, x_0. The latter two were calculated for each slope angle considered using a simple linear fit to the top of the head at two locations and then extrapolating to zero height (figure 1). The results are shown in figure 3. The entrainment coefficient can be calculated from the spread rate, α_0, through equation (4), and compared to the entrainment coefficients found by Beghin *et al.* (1981). Our entrainment coefficients tend to be slightly smaller than the average values of Beghin *et al.* (1981) ranging from 60 %, for a slope of 5°, to 80 %, for a slope of 15°.

The video records, such as that in figure 2, were carefully analysed to determine the location of the front edge of the current. A typical history is given in figure 4. In this figure, note that the data between $x = 0$ and 20 cm has not been plotted (x is the distance from the lock gate to the front edge of the current head). This is the result

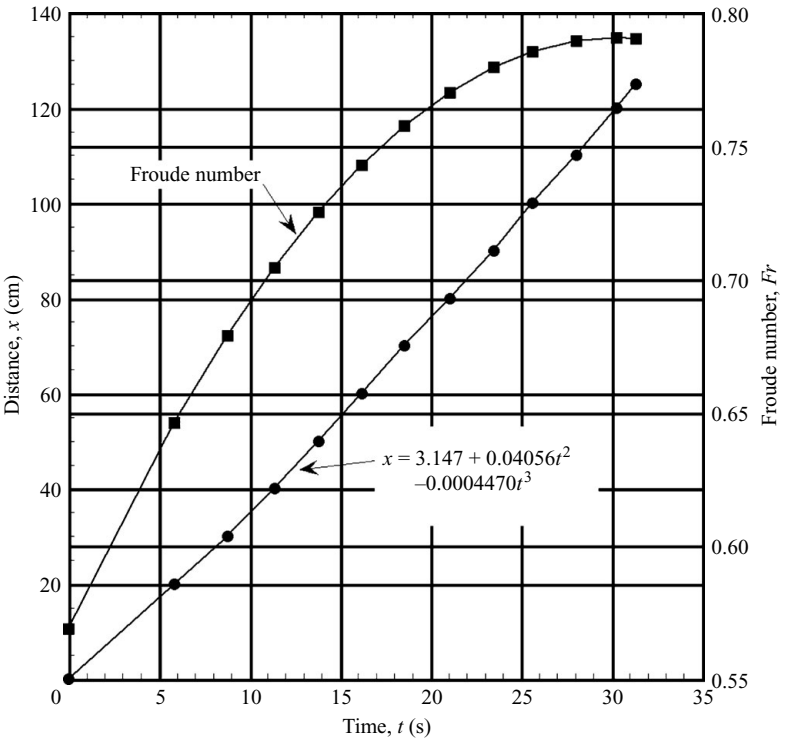

FIGURE 4. Raw data, x *vs.* t and Fr_h *vs.* t for experiment 19/4/05-3. $\theta = 13°$, $g' = 3.06\,\mathrm{cm\,s^{-2}}$, $(g'H_0)^{1/2} = 5.53\,\mathrm{cm\,s^{-1}}$.

of the observation that the initial motion was consistently different from case to case, presumably because of the different turbulence scale and magnitude generated by the opening of the lock gate. Thus, the equation for the front location, given on the graph and below, applies only to that portion beyond $x = 20\,\mathrm{cm}$ while the fictitious initial velocity is simply that found by curve fitting at $x = 0$.

In all but a few cases, a cubic polynomial fit the trajectory of the front edge of the current to a high degree of accuracy. Thus,

$$x = m_0 + m_1 t + m_2 t^2 + m_3 t^3, \tag{8}$$

with m_0 very small. To be consistent with the theory of Beghin *et al.* (1981), interest is mainly in the velocity history of the motion, so differentiating (8) yields

$$U_h = m_1 + 2m_2 t + 3m_3 t^2, \tag{9}$$

where U_h is the velocity of the leading edge of the head. The quantities in this equation can be made dimensionless using the velocity scale $(g'H_0)^{1/2}$ and time scale $(H_0/g')^{1/2}$. Thus, (9) becomes:

$$Fr_h = Fr_{h0} + A_0 T + D_0 T^2, \tag{10}$$

where $Fr_h = U_h/(g'H_0)^{1/2}$ is the running internal Froude number of the leading edge of the head; $Fr_{h0} = m_1/(g'H_0)^{1/2}$ is the initial internal Froude number, $A_0 = 2m_2/g'$ is an acceleration parameter or number, $D_0 = 3m_3/(g'^3/H_0)^{1/2}$ is a deceleration parameter (which is negative) and $T = t(g'/H_0)^{1/2}$.

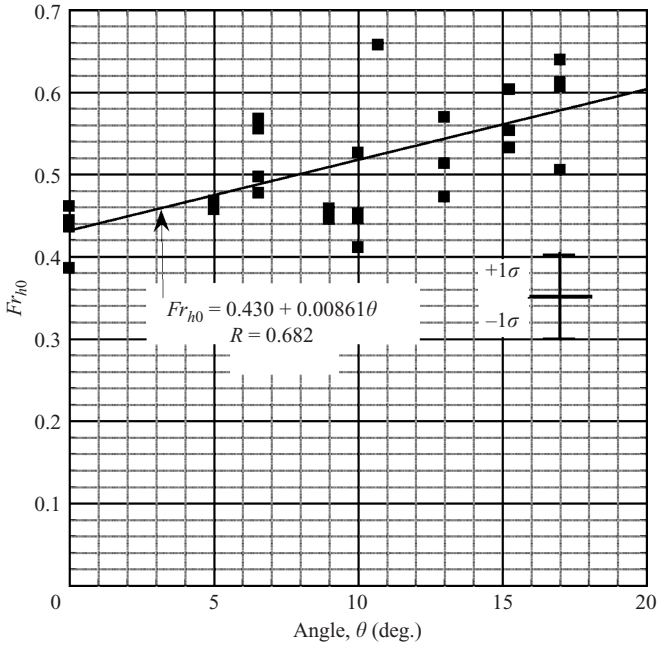

FIGURE 5. Fr_{h0} *vs.* θ, $H_0/L_0 = 0.5$. The error bars indicate one standard deviation for the average straight-line fit.

Based on the results from approximately 30 experiments, figures 5 to 7 show the dependence of Fr_0, A_0 and D_0 on the angle of the channel to the horizontal, θ. The value of Fr_0 for $\theta = 0^\circ$ is close to the available values for the flat-bottomed case, whereas figures 6 and 7 show that the acceleration/deceleration parameters in that limit are close to, but not, zero.

What is clear from these figures is the high degree of variability between experimental runs with the same slope angle. This variability is not typical of gravity currents on a horizontal surface, as can be seen from the reduced spread in the Fr_0, A_0 and D_0 parameters for the case of $\theta = 0$ (a point that has been made by others, e.g. Shin, Dalziel & Linden 2004). This variability is not due to experimental error; it is an intrinsic characteristic of these flows. A non-zero slope leads to a more vigorous current than is achieved for the horizontal case. The heads of these energetic currents are unstable and apparently slightly different turbulent evolutions can lead to sizeable differences in the x *vs.* t history. Subtle differences in the initial conditions, caused by the extraction of the gate, also may be amplified by the large-scale turbulent structure that develops downstream.

Based on the curve fits shown in figures 5 to 7, we can reconstruct average velocity profiles as functions of both $X = x/H_0$ and T, realizing that there can be substantial deviations from these. In particular, the large scatter in A_0 and D_0 means that the maximum of Fr can occur over a wide range of X, although, for the averaged parameter values, the position of the maximum is almost constant. However, there is some value to plotting typical curves (figure 8) to give some indication of the variations with angle. Note that the maximum of Fr_h is reached just before the end of the channel and that the very broad maximum could easily be interpreted as a region of constant Fr_h. This is particularly true when viewing the raw x *vs.* t plots where it is easy to misinterpret the region around the inflection point as having a constant

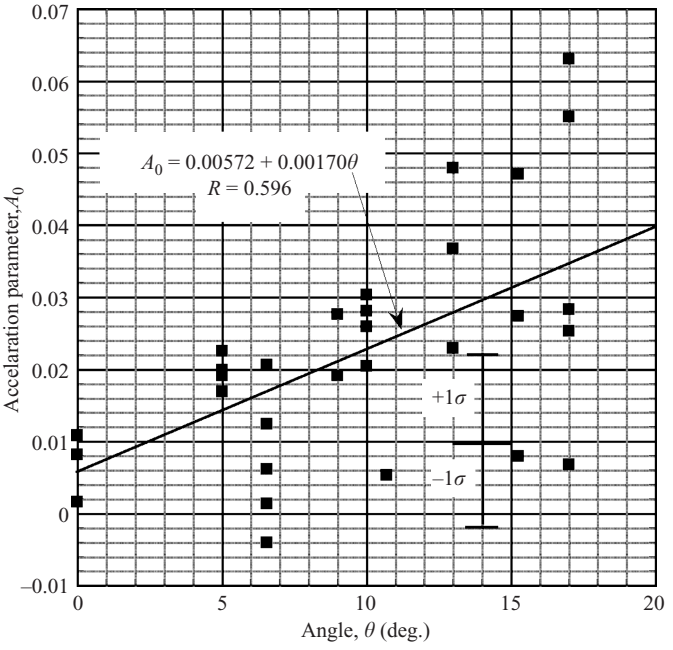

FIGURE 6. Dimensionless acceleration parameter, A_0 *vs.* θ, $H_0/L_0 = 0.5$. The error bars indicate one standard deviation for the average straight-line fit.

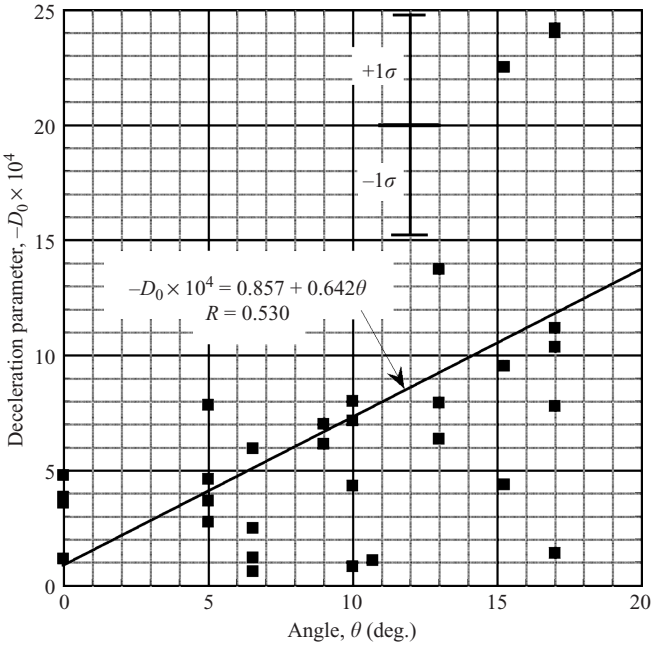

FIGURE 7. Dimensionless deceleration parameter, $-D_0 \times 10^4$ *vs.* θ, $H_0/L_0 = 0.5$. The error bars indicate one standard deviation for the average straight-line fit.

velocity. There is some disagreement over using a straight-line fit to the data, since Fr_{h0}, at least, must have a maximum at some larger angle than that used here. Given the large scatter, this seems to be the most honest way to treat the data, any other

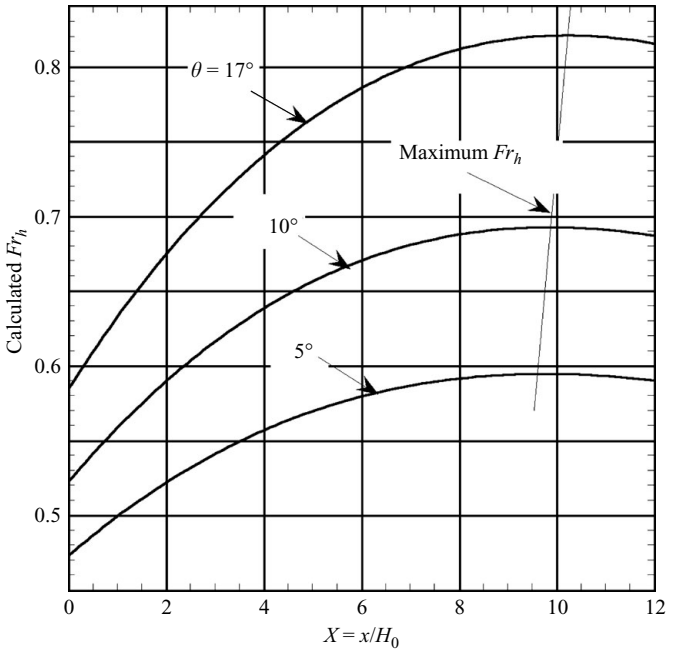

FIGURE 8. Calculated plots of Fr_h *vs.* X using the fit values of Fr_{h0}, A_0 and D_0 from figures 5 to 7, for three values of channel slope. $X = 12$ represents the end of the experimental channel.

method giving results for averaged plots of x *vs.* t that are well within experimental error.

Figures 3 and 8 allow for some interesting comparisons with Beghin *et al.* (1981) and to some extent with Laval *et al.* (1988). The model of Beghin *et al.* (1981) predicts that the current head will enter its deceleration phase at $x_{CoM} = 0.59x_0$ if the current starts from rest. Based on the measured parameters given in figure 3, the deceleration phase should exist well within the length of the present channel, not near the end, as illustrated in figure 8. The only slightly questionable case is that for $\theta = 5°$ for which deceleration is predicted to start beyond approximately $x_{CoM} = 91$ cm or $X = 11$. In practice, the deceleration phase is likely to begin even earlier. As the fluid within the lock does not begin its motion with the self-similar form assumed in the model, the position of the virtual origin, and the start of motion, are defined from the point at which the front of the current is approximately 2 lock depths downstream of the gate (see figure 1). Thus, the current will be correctly modelled as having a non-zero initial velocity, or Fr, as illustrated in the solutions discussed in § 4. The consequence of this is to move the point of maximum velocity closer to the gate.

The video sequences, and direct observations of the flow, suggest that the major cause of the extended acceleration phase is due to the aspect ratio (H_0/L_0) of the lock in the present study being considerably smaller than that of Beghin *et al.* (1981). This can be anticipated from figure 2(*a*) where the head of the current is formed by only a small fraction of the total volume of fluid within the lock, approximately 60 cm^2 in this case. The majority of the contents of the lock, 140 cm^2, continues to feed the head as it progresses down the slope.

It is apparent that if the aspect ratio of the lock were large enough, then once the fluid is released by the gate, the vast majority of the fluid within the lock exits

as part of the current head, and little fluid is left to feed the head from behind. Thus, the assumption of constant buoyancy within the head, as invoked in the model, is approximately valid. On the other hand, for small-aspect-ratio locks, only the portion of the fluid closest to the gate will compose the head of the current, leaving a significant volume of the original fluid behind in the tail. This fluid can feed additional buoyancy into the head as it propagates downslope. For this reason, it seems likely that the experimental results of Beghin *et al.* (1981) indicate a short acceleration phase, consistent with their model, whereas ours do not.

The results of Laval *et al.* (1988) are somewhat more difficult to interpret. They used several different initial volumes, but the aspect ratio of their lock is not clearly described. In addition, only results for very small angles, 3° or less, are presented in the paper, and it is generally believed that the flows generated on angles of less than 5° tend to resemble those on a horizontal bottom boundary more than those on steeper angles.

3. Flux experiments

3.1. *Apparatus and experimental procedures*

A series of experiments were carried out with the aim of quantifying the flux of buoyancy entering the head of the current as it propagates away from the gate. This was achieved by measuring fluid velocities within the current and surrounding fluid, along the length of the channel. *Fluidstream* 6.01, an optimization-based implementation of a particle tracking velocimetry (PTV) system, developed at the University of Canterbury (see Nokes 2005), was employed to measure the fluid velocities.

Prior to the start of an experiment both the undyed salt solution within the lock, and the ambient fresh water, were seeded with pliolite VT resin particles, with diameters in the range 180–250 μm. For the time scale of these experiments, these particles can be treated as neutrally buoyant. The particles were illuminated by a white light source comprising a linear 2 kW halogen bulb encased within a heat resistant box. The light from the bulb passed through two narrow slits, approximately 5 mm wide × 400 mm long. The resulting white light sheet was approximately 10–15 mm in width and slightly diverging in a direction perpendicular to the sheet. From our experience, for relatively small experimental flow domains, the uniformity of this light sheet is adequate for PTV measurements of essentially two-dimensional flows, and has the advantage over laser sheets of being cheap, and easy to produce.

A JAI CV M4 + CL digital video camera with resolution 1268 × 1024 pixels running at 24 Hz was used to record the motion of the pliolite particles. The camera was fixed on a tripod and angled so that the camera frame was aligned with the channel slope.

The *FluidStream* software produced two-dimensional velocity fields from the recorded images. Initially, particles were identified in each image based on threshold light intensities. These particles were matched from frame to frame using an optimization technique based on a number of different costing strategies. The resulting matches were checked for consistency. Finally, a two-dimensional velocity field was produced for each image based on the particle matches in that image. The velocity field was interpolated onto a rectangular grid using a Thessian triangulation technique.

Because of the small aspect ratio (depth to length) of the channel and the desire to have reasonably detailed velocity data, it was impossible to measure velocities along the entire channel in one experimental run. Therefore, four experimental runs were performed for each channel slope. In each run, the camera was moved to a different location, so that the region extending from 2 lock depths to 10 lock depths

downstream of the gate was covered in the four runs. The flow domain in each run covered slightly more than 2 lock depths along the channel, thus ensuring some overlap between runs. Slope angles of 0°, 5°, 9.5°, 13° and 17° were investigated.

3.2. *Results*

For each PTV run, the average *Fr* of the front was calculated as a check for consistency with the dye-based experiments. The front speed was deduced in two ways. First, the raw particle images were analysed and the time taken for the front to travel from one side of the camera window to the other was determined. This measurement is not as easy with particle images as it is with dye images, as the location of the front can be difficult to determine. For this reason, a second method was devised. Using the velocity field data, a contour plot of the vertical (or horizontal) component of the velocity field at a fixed height in the flow (typically $0.1H_0$) was plotted as a function of x and t. The front appears as a characteristic curve in the (x, t)-plane which is generally easily identified, and the average slope of this characteristic was used as a second estimate of the front speed. These two estimates generally agreed to within 5 %.

The Froude numbers derived from the PTV experiments exhibited the same variability as those from the dye experiments when the slope angle was 5° or greater – with differences between the canonical curves in figure 8 and those calculated from the PTV experiments typically within ± 15 %. Once again, for a horizontal bottom, this variation was minimal and the Froude numbers for the four runs at this angle agreed to within a few per cent. The impact of this variability is that velocity fields from different runs at the same slope cannot be directly compared or overlaid, and hence the deduced buoyancy, or volume, fluxes are hard to interpret.

To resolve this problem, the velocity fields for each run were non-dimensionalized using the same space, time and velocity scales as introduced earlier, and then scaled so that the Froude number computed from the velocity field at the mid-point of the measurement window matched the *Fr* at the same location on the 'canonical' *Fr* curve found in figure 8. Thus, if the measured *Fr* was lower than that in figure 8, then all velocities in the measured field were increased by the appropriate factor. Following the scaling of the velocity fields, time scales were also transformed to ensure consistency in the non-dimensional coordinates. Finally, the temporal and spatial coordinates for all runs, at a particular slope, were translated to ensure that the coordinate systems of all runs could be overlaid.

While this approach is not ideal, as it ignores changes in flow structure between runs, it at least provides a consistent way of analysing the velocity data.

This transformed velocity data was used to provide an estimate of the inflow of negatively buoyant material from the following current into the head. The head can be viewed as a fluid volume that expands as it moves downslope. The theory of Beghin *et al.* (1981), and our measurements, indicate that both the height and length of the head increase approximately linearly from a virtual origin. For fluid in the following current to be able to enter the head, and hence contribute to its overall buoyancy, it is reasonable to require that its velocity should exceed that of the trailing edge of the head. Certainly, fluid travelling towards the front at a speed of less than the trailing edge will be left behind in its wake. The speed of the trailing edge was not measured experimentally. Instead, this speed was calculated from the measured front speed, the growth rate of the head and its aspect ratio. For all calculations here, variations in the aspect ratio were ignored and a constant aspect ratio of 0.25 was assumed, although observations suggest that near the gate, the aspect ratio is somewhat larger than this.

In order to calculate the buoyancy flux into the head, two assumptions were made. First, any material entering the head from the following current was assumed to have the same density as the fluid initially within the lock. This allows volume fluxes, that can be obtained from the velocity data, to be readily converted into buoyancy fluxes. Without actual concentration profiles, this assumption cannot be strictly justified. However, it seems reasonable to believe that fluid that has been significantly diluted through entrainment and mixing at the interface between the ambient and dense fluids will possess insufficient downslope momentum to keep pace with the head. Secondly, the volume flux into the head is calculated at the location behind the head where the following current depth is a minimum. This depth is found by determining the height above the slope at which the velocity in the flow drops below the velocity of the trailing edge of the head. This second assumption is made for two reasons. (i) An unambiguous location for calculating the flux must be determined, and it was found, almost without exception that a clear minimum depth occurred within the following current close to the rear of the head. (ii) Visual inspection of the velocity fields indicated that this minimum depth occurred roughly at the rear of the head (although the definition of the head in unsteady flows of this nature is often difficult). A comparison between the position of minimum depth and the location of the rear of the head calculated from the front position, and L calculated from the growth rate of the head, were generally in good agreement, although as mentioned above, near the gate the latter of these two estimates tended to predict a position that was further upslope. In other words, the minimum depth location tended to suggest that the aspect ratio of the head was larger than 0.25 near the gate.

Figure 9 illustrates a typical longitudinal profile of the current depth (as defined above) at $T = 8$ for a slope angle of 9.5°. A minimum depth at $X \sim 3.1$ is identifiable in figure 9(*a*) and this location clearly corresponds to the narrow inflow at the rear of the current head (figure 9*b*).

The two-dimensional volume flux into the head was calculated as the integral, over the minimum depth, of the current velocity that is in excess of the trailing edge velocity. Flux calculations could not be made in the early period of propagation. During this time, the current was becoming established and initially, at least, the trailing edge of the current was within the lock or just downstream of the gate, where velocity measurements were not taken. Therefore, flux measurements began when the current head was approximately 4 to 5 lock depths from the gate.

The scatter in the calculated fluxes is significant (see figure 10), owing to the turbulent nature of the flow, and the fact that the fluxes are obtained from instantaneous velocity profiles. Nevertheless, the fluxes show a clear decrease beyond approximately 6 lock depths from the gate, vanishing when the current head is between 11 and 14 lock depths downstream. Before this region of decreasing flux there is a suggestion that the flux is approximately constant, and this assumption will be made here. Certainly for lock exchange flows on a horizontal surface, the volume flux from the lock is approximately constant until the finite length of the lock is felt (McBryde 2006) and this would add some support to such as assumption in the early stages of the current's development.

For each slope, three parameters were used to fit the flux data. The first is the initial constant flux, the second the value of X at which the flux begins to decrease, X_T, and the third is the value of X at which the flux becomes zero, X_Z. The first of these parameters was estimated from the limiting flux values near the transition, while the second and third were found from a least-squares linear fit to the flux data beyond the constant region. All three parameters are given in table 1.

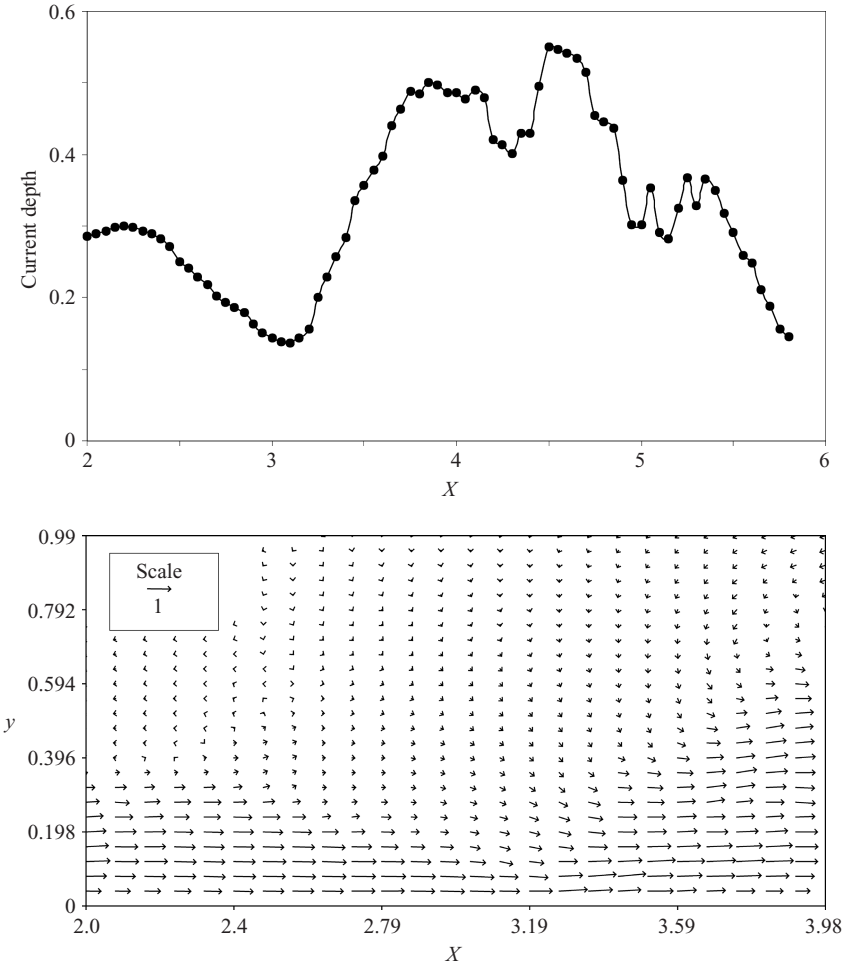

FIGURE 9. (*a*) The current depth as a function X for $T = 8$ and a slope angle of 9.5°. The inflow depth is defined as the minimum current depth closest to the current head, where the current depth is defined as the height within the flow where the flow velocity first drops below the trailing-edge velocity. The data in this figure were obtained by overlaying two different runs. The overlap occurs between $X = 3.8$ and $X = 4.2$. (*b*). The velocity field corresponding to $T = 8$ for a slope angle of 9.5°. The minimum depth corresponding to the inflow depth in (*a*) can be identified at $X \sim 3.1$.

The fluxes for all runs are presented in figure 10. In this figure, the flux has been scaled by its value in the constant region, and X has been scaled by the point at which the flux vanishes. Although alternative fits could be suggested, those used here tend to capture the key features of the flux, and the final solutions tend to be relatively insensitive to the exact form of the flux functions, particularly in the linear decay region where the contribution to the total flux is less significant.

Clearly, at some point, the following current will no longer be able to feed the head. Either it will exhaust the supply of material from the lock, or the head (which is still accelerating at this time) will be travelling too rapidly for the following current, which is gradually thinning with distance along the slope, to keep up. The results above indicate that the distance at which the feed ceases is almost independent of

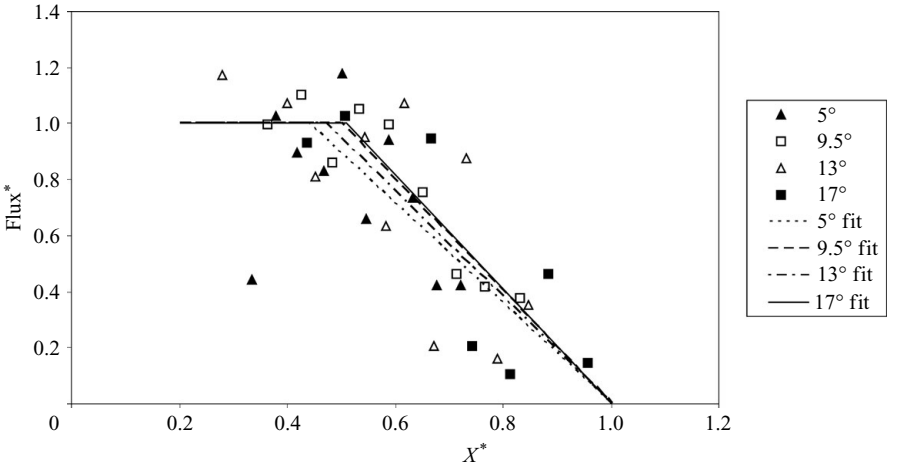

FIGURE 10. The inflow volume flux as a function of front position for slope angles 5°, 9.5°, 13° and 17°. The flux has been scaled with the initial constant flux, and X has been scaled by the point at which the flux is estimated to vanish. These quantities are given in table 1. Note the constant flux portion of the curve only extends to the initial position of the motion, which corresponds to approximately $X = 2$.

θ (deg.)	k	Flux	X_T	X_Z	β_I	V_I	$\Delta\beta$	ΔV	$\Delta\beta/\Delta V$
5	0.25	0.028	6.9	12.8	0.67	0.92	0.36	1.64	0.22
9.5	0.25	0.05	5.7	11.9	0.64	0.95	0.51	2.41	0.21
13	0.25	0.046	6.2	13.9	0.62	0.79	0.51	3.54	0.14
17	0.25	0.075	5.7	11.6	0.69	1.09	0.62	3.24	0.19

TABLE 1. Variable buoyancy model parameters. θ is the slope angle; k is the aspect ratio $= H/L$; flux is the estimated constant flux; X_T is the downstream location of the current's leading edge at which point the flux begins to decay; X_Z is the downstream location of the current's leading edge at which the flux drops to zero; β_I is the initial dimensionless buoyancy (volume) within the head; $\Delta\beta$ is the change in dimensionless buoyancy (volume) owing to the inflow from the following current; V_I is the initial dimensionless (volume) within the head calculated from H and L at the start of the motion; ΔV is the total change in dimensionless head volume deduced from the calculated values of H and L (evaluated at the point where the flux from the following current ceases), it includes the increase in volume owing to the following inflow and entrainment. Thus, $\Delta\beta/\Delta V$ is the proportion of the total flow into the head owing to the flux from the following current. Note, β_I is found from a best-fit match between the experimental and model curves and $\Delta\beta$ is found from the integral of the measured buoyancy flux (see (15)).

angle, and is between 11 and 14 lock depths from the gate. Table 1 shows a flux dependence on slope, with the initial flux increasing with slope angle. Although there is little difference between this initial value for the 9.5° and 13° slopes, an overall trend is clearly evident. Although the *Fr* of the front increases significantly with slope angle (see figure 8), the *Fr* of the trailing edge does not, owing to the increase in growth rate with slope angle. Thus, as the flow velocities increase with slope angle so does the volume flux.

4. Theoretical model

Beghin *et al.* (1981) modelled the motion of the centre of mass (CoM) of an isolated volume of fluid driven down a slope by its inherent negative buoyancy as discussed in § 1. This buoyancy was gained at the time of release and was assumed to remain constant. The model predicted a brief initial acceleration phase followed by a deceleration due to the entrainment of ambient fluid. Our experiments exhibit significantly different behaviour where the acceleration phase continues until the front reaches a distance of approximately 10–11H_0 from the lock gate. The flux measurements of the previous section suggest that this extended period of acceleration results from the continual feeding of negatively buoyant material into the rear of the head during the initial phase of its motion. In this section, we explore the implications of increasing buoyancy on the Beghin *et al.* (1981) model. In addressing this problem, we will use the experimental flux results of the last section as an input to the model. Note that Rastello & Hopfinger (2004) presented a model where increasing buoyancy due to entrainment of snow from the bottom boundary was included. Although the mechanism by which the buoyancy increases is different, the qualitative effect on the motion of the current head will be similar.

The theory of Beghin *et al.* (1981) was briefly reviewed in § 1. We now generalize this by writing (1) as

$$\frac{\mathrm{d}(\rho_A(1+k_v)S_1HLU)}{\mathrm{d}t} = B(x_{CoM})\sin\theta, \tag{11}$$

where $B(x_{CoM})$ indicates that the buoyancy is now a function of the position of the centre of mass. Using the expressions for L and H derived by Beghin *et al.* (1981) (11) can be converted into an ODE for U as a function of x_{CoM} given by

$$U\frac{\mathrm{d}\left(x_{CoM}^2U\right)}{\mathrm{d}x_{CoM}} = \frac{4B(x_{CoM})S_1\sin\theta}{S_2^2\alpha^2(1+k_v)\rho_A}. \tag{12}$$

Note that the solution of (12) yields a constant velocity when the buoyancy within the head grows linearly with x_{CoM}. This is the constant flux problem considered by Britter & Linden (1980) and their results provided clear evidence of this constant velocity regime.

Non-dimensionalizing the velocity and length scales with $\sqrt{g'H_0}$ and H_0, respectively, yields the equation for the centre of mass Fr given by

$$Fr\frac{\mathrm{d}\left(X_C^2Fr\right)}{\mathrm{d}X_C} = \beta(X_C)\frac{4S_1\sin\theta}{S_2^2\alpha^2(1+k_v)}, \tag{13}$$

where $X_C = x_{CoM}/H_0$ and β is a dimensionless volume in units of H_0^2 defined by

$$B = \beta g'\rho_A H_0^2. \tag{14}$$

If the buoyancy within the head is equal to that initially in the lock, then $\beta = L_0/H_0$. β can be calculated using the flux measurements described previously

$$\beta = \int_{x_0/H_0}^{X_C}\mathrm{Flux}\,\mathrm{d}t + \beta_I = \int_{x_0/H_0}^{X_C}\mathrm{Flux}(X_C)\frac{\mathrm{d}t}{\mathrm{d}X_C}\mathrm{d}X_C + \beta_I = \int_{x_0/H_0}^{X_C}\frac{\mathrm{Flux}(X_c)}{Fr}\mathrm{d}X_C + \beta_I, \tag{15}$$

where β_I is the initial buoyancy within the head at $X_C = x_0/H_0$. Note that the integral in (15) is with respect to the position of the centre of mass, X_C, not the front location which was used in the previous section to present the flux data. Strictly speaking,

the integral in (15) cannot be evaluated without knowledge of the Froude number of the centre of mass. However, to simplify matters, we will use an average value for *Fr* taken from the experimental data. Although *Fr* varies by as much as 20 % from the average value, we do not believe the errors introduced are significant relative to those from the flux measurements themselves.

One piece of information that is required in evaluating β is the initial volume of buoyant material within the head of the current, β_1. This can be estimated in a number of ways. Ideally, it could be deduced from the dye experiments, but such estimates are likely to incur relatively large errors. Alternatively, it could be determined by matching the initial slope of the experimentally determined *Fr* curve with that of the model. However, this approach is also problematic as it is in the near-gate region that the model is most likely to deviate from the observed behaviour owing to an initial transient phase in which the self-similar form of the head fully develops and the conditions at release are forgotten. Instead we choose an initial buoyancy that yields the best fit between model and experiment. These initial values are presented in table 1 along with the increase in volume, $\Delta\beta$, obtained from the integral in (15).

Table 1 also gives the contribution made to the total inflow into the head by the flux from the following current – the remainder of this inflow being due to the entrainment expressed in (3). This contribution is calculated at the point on the slope at which the flux from the following flow terminates. The figures indicate that while the inflow through the rear of the head is significant, around 20 % of the total inflow, the dominant contribution to the head growth still comes from the turbulent entrainment through the head/ambient interface. The assumption of self-similarity that is intrinsic to the entrainment model embodied in (3) is clearly not valid for the inflow from the following flow. However, this lack of self-similarity does not appear to have a major effect on the overall growth of the head, which exhibits a near linear growth with distance. If the effect of the inflow were to be detected it is most likely to be seen near the gate where the head is small and the motion slow. Table 1 also shows that the initial buoyancy captured within the head is roughly independent of slope angle, while the total buoyancy fed into the head increases markedly with angle.

Although (15) can be integrated directly if $\beta(X_c)$ can be written as a polynomial, it is simpler to integrate it numerically for each slope angle, using the piecewise linear flux functions to evaluate $\beta(X_c)$. Figure 11 presents the results of these integrations for two slope angles, 9.5° and 17°. These two slopes represent the best and worst fits between the model predictions and experimental results. Plotted in each figure is the experimentally determined dependence of *Fr* on *X* (for the front, tail and centre of mass of the head), the variable buoyancy model predictions, and two different scenarios based on the constant buoyancy model given in (4). A different buoyancy is used in each of these scenarios. In model 1, the total buoyancy matches the initial buoyancy in the variable buoyancy model, β_1, and in model 2, the total buoyancy initially within the lock is used, i.e. $\beta = 2$. Note that the models are not started from rest, for the reasons discussed in § 2.2. Instead, the *Fr* is given an initial value that matches the experimental curves.

The results demonstrate that the constant buoyancy model is unable to reproduce the trends observed in the dye experiments. The most prominent feature of the experimental curves, as discussed previously, is the continual acceleration of the head, until it reaches approximately 10 or so lock depths from the release point. The constant buoyancy model predicts a maximum *Fr* much closer to the gate, this maximum occurring further upstream as the slope increases, or the buoyancy decreases. Thus, for an angle of 17°, with a buoyancy of β_1, the maximum *Fr* occurs

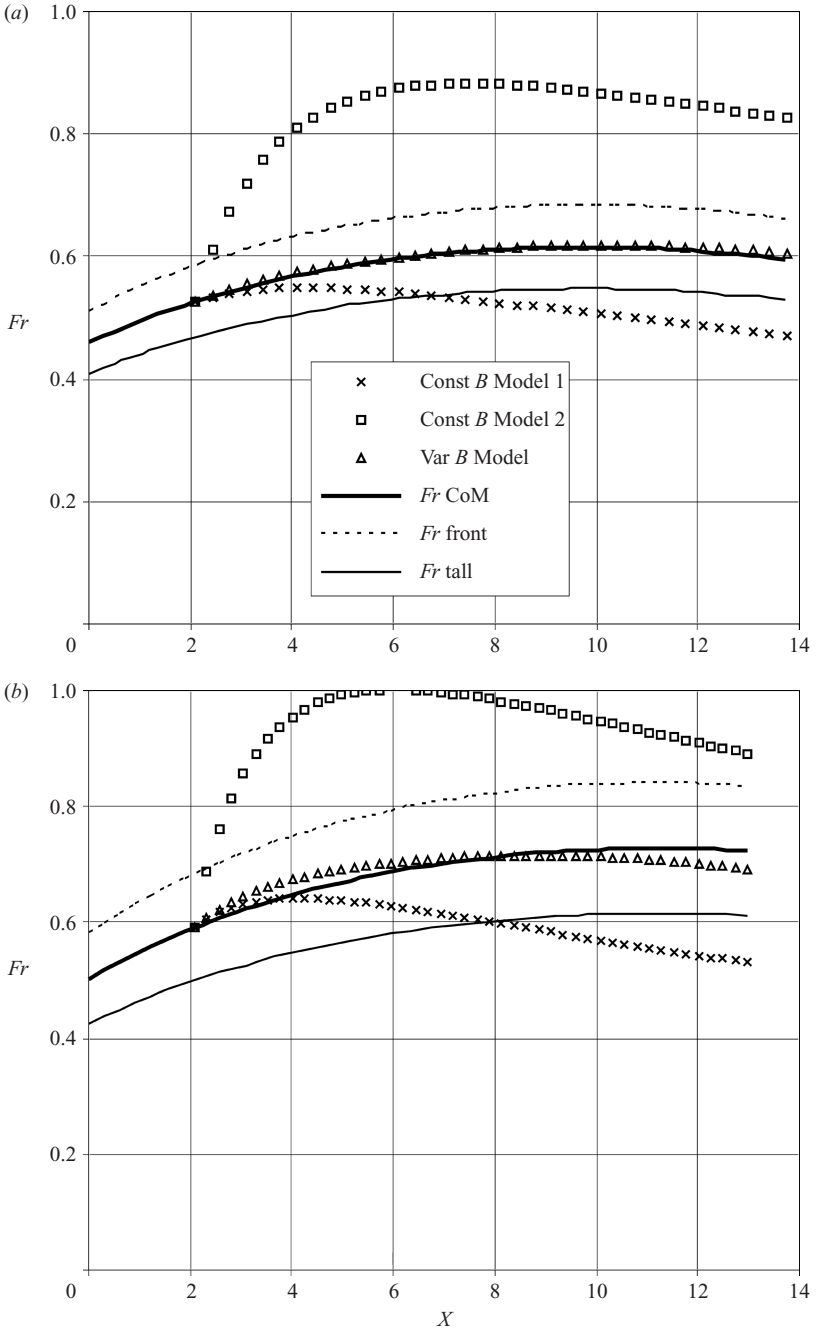

FIGURE 11. The *Fr* of the centre of mass, tail and front, as functions of the front position for (*a*) 9.5° and (*b*) 17°. The dashed line corresponds to the *Fr* of the front determined from the dye experiments, while the dark and light solid lines correspond to the centre of mass and tail Froude numbers, respectively. The other symbols correspond to model predictions based on constant or variable buoyancy within the head (as explained within the text). Note the model curves begin at the initial position of the motion, which corresponds to approximately $X = 2$.

at approximately 3 lock depths downstream of the gate. Only for the 5° slope, with the total buoyancy in the lock contained within the head, does the location of the maximum *Fr* approach $X \sim 10$. In addition, the constant buoyancy model either predicts substantially higher *Fr* values than those seen in the laboratory data, when a larger buoyancy value is selected, or it leads to unrealistically low speeds downstream when a lower buoyancy is assumed.

In contrast, the variable buoyancy model, despite its crudity, is surprisingly successful at predicting the evolution of *Fr*. The extended acceleration phase is present in the predictions for all angles, and the general trend of the experimental curves is faithfully reproduced by the model. For the lower angle, 9.5°, the agreement between experiment and model is very good throughout the region of measurement. For the largest slope, 17°, the model curve tends to overpredict the speed of the centre of mass initially and underpredict it as the current approaches its maximum speed. The results for 13° exhibit the same trend, although to a lesser degree than for the 17° case. This may suggest that the assumption of a constant flux early in the current's development is less appropriate for the larger angles than it is for the smaller angles. Even so, to reproduce the latter portion of the motion, the flux would need to last longer, and at a higher level than that predicted by the measured fluxes.

All of these variable buoyancy model curves are based on the choice of an initial buoyancy that leads to the best fit between the model and experimental curves. Increasing this initial buoyancy increases the *Fr* throughout the motion, whereas decreasing it leads to the opposite effect.

While the agreement between model and experiment is somewhat less convincing with increasing angle, these results support the notion that the incorporation of a buoyancy flux into the rear of the head, during its initial development, is critical in predicting the motion of the head.

5. Discussion of the results in the initial acceleration phase

Based on the observations and results presented above, the dynamical processes involved in the motion of a gravity current down a slope now seem clearer. After the lock gate was suddenly opened, a lower layer with a more or less constant thickness, at slightly more than half the lock height, was formed. This rapidly evolved into an approximately semi-elliptically-shaped head with an initial aspect ratio (H/L) of between 0.25 and 0.30 containing a fraction of the fluid originally in the lock. The larger fraction of the lock fluid acted as a feeder layer, with decreasing flux, into the rear of the head, and resulted in a steadily increasing negative buoyancy driving the downward motion until, at, or close to, the maximum velocity, the inflow ceased. After the flux of negatively buoyant fluid into the current head ceased, it could be assumed, as has been done by previous workers, that the current would then propagate as a current with constant buoyancy, i.e. with a velocity that eventually decreases as $X_B^{-1/2}$ or $T^{-1/3}$. However, the present channel was not long enough for that state to be reached. Experiments in a longer channel that explore the modification of such a decay law for a variety of geometries will be presented in Part 2 (Maxworthy 2007*a*).

Using knowledge gained to this point, we might predict that if the lock length (L_0) had been sufficiently small, the initial head could have contained most, if not all, of the lock fluid, and the case considered experimentally, and theoretically, by Beghin *et al.* (1981) would have been rapidly achieved. An estimate of this length for the present geometry is in the range 6–12 cm. We can apply a variation of this argument to the data in Beghin *et al.*'s figure 9, for example. Their H_0 was 8 cm, so we can

estimate that the initial outflow layer was approximately 4.2 cm deep. Assuming that the aspect ratio of the initial head was 0.26, as for the present 9° case, then $L = 16$ cm and its volume 53 cm^2. The lock volume was 80 cm^2 so only 27 cm^2 would be available to feed the head. We suspect that this might be one of the reasons for the slight discrepancy in their experimental and theoretical comparison.

The results of Laval *et al.* (1988) must also be re-evaluated, although here there is some difficulty since they did not present all of the data and conditions that are required for a completely satisfactory discussion. Based on their sketch of the apparatus, it seems that the saline solution never filled the lock, thus the initial outflow was most probably the same height as the initial static height, as found in Part 2 (Maxworthy 2007*b*) of the present series. Based on this assumption, and using a value of $k = 0.25$, we can estimate the volume of the initial head and show that all but the lowest initial height had a volume that included almost all of the lock fluid. Therefore, these should quickly evolve as constant buoyancy currents: as they, in fact, found. The shallowest initial depth was of the type discussed in our experiments, but no detailed measurements were presented of that case. Also, since all their experiments appeared to use a constant lock length, their finding of a velocity variation with the square root of the volume could be interpreted, as here, as a variation with $H_0^{1/2}$.

6. Conclusions

A laboratory study of gravity currents in sloping open channels, generated by the release of a finite volume of dense fluid from an enclosed lock, has been described. The results from approximately 30 visual dye experiments, for slope angles ranging from 0° to 17°, clearly indicate that the current head does not exit the lock with its entire initial buoyancy content when the lock aspect ratio is equal to 0.5. Velocity measurements, obtained from a series of PTV experiments, confirm our visual observations that, until the current head reaches approximately 12 lock depths downstream of the gate, it is fed from behind by a dense current comprising some of the fluid left behind in the lock. This buoyancy flux explains the extended acceleration period observed in our experiments when compared to the predictions of a constant buoyancy model developed by Beghin *et al.* (1981). This model has been adapted to account for increasing buoyancy within the head, and using buoyancy flux estimates deduced from the velocity measurements, good agreement between the experimental *Fr* time histories and the model predictions has been obtained.

T. M. wishes to thank the members of the Department of Civil Engineering at the University of Canterbury for their hospitality during a two and a half month stay in early 2005. Special thanks go to Ian Sheppard and Kevin Wines, the lead technician and technician, respectively, in the Fluid Dynamics Laboratory, for their expert help in constructing the apparatus and making the day-to-day operation run smoothly.

REFERENCES

Alavian, V. 1986 Behavior of density currents on an incline. *J. Hydraul. Engng ASCE* **112**, 27–42.

Beghin, P., Hopfinger, E. J. & Britter, R. E. 1981 Gravitational convection from instantaneous sources on inclined boundaries. *J. Fluid Mech.* **107**, 407–422.

Birman, V. K., Battandier, B. A., Meiburg, E. & Linden, P. F. 2007 Lock-exchange flows in sloping channels. *J. Fluid Mech.* **577**, 53–77.

Britter, R. E. & Linden, P. F. 1980 The motion of the front of a gravity current travelling down an incline. *J. Fluid Mech.* **99**, 531–543.

Dade, W. B., Lister, J. R. & Huppert, H. E. 1994 Fine-sediment deposition from gravity surges on uniform slopes. *J. Sed. Res.* A **64**, 423–432.

Ellison, T. H. & Turner, J. S. 1959 Turbulent entrainment in stratified flows. *J. Fluid Mech.* **6**, 423–448.

Escudier, M. P. & Maxworthy, T. 1973 On the motion of turbulent thermals. *J. Fluid Mech.* **61**, 541–552.

Etienne, J., Hopfinger, E. J. & Saramito, P. 2006 Numerical simulations of non-Boussinesq clouds on sloping boundaries. *J. Fluid Mech.* (submitted).

Georgeson, E. H. M. 1942 The free streaming of gases in sloping galleries. *Proc. R. Soc. Lond.* A **180**, 484–493.

Hopfinger, E. J. & Tochon-Danguey, J. C. 1977 A model study of powder-snow avalanches. *Glaciology* **19** (81), 343–356.

Kersey, D. G. & Hsu, K. J. 1976 Energy relations of density-current flow: an experimental investigation. *Sedimentology* **23**, 761–789.

Laval, A., Cremer, M., Beghin, P. & Ravenne, C. 1988 Density surges: two-dimensional experiments. *Sedimentology* **35**, 73–84.

Luthi, S. 1981 Some new aspects of two-dimensional turbidity currents. *Sedimentology* **28**, 97–105.

McBryde, J. 2006 Experimental and numerical modelling of the effects of compartment opening geometry on the mixing in gravity currents preceding backdraft. MEFE thesis, *University of Canterbury*, to be submitted.

Maxworthy, T. 2007(*a*) Experiments on gravity currents propagating down slopes. Part 2. The evolution of a fixed volume of heavy fluid released from closed locks into a long, open channel. In preparation.

Maxworthy, T. 2007(*b*) Experiments on gravity currents propagating down slopes. Part 3. Release of a fixed volume of a particle-laden fluid, without and with buoyancy reversal. In preparation.

Nokes, R. I. 2005 *FluidStream Version 6.01 – System Theory and Design*. University of Canterbury 68.

Rastello, M. & Hopfinger, E. J. 2004 Sediment-entraining suspension clouds: a model of powder-snow avalanches. *J. Fluid Mech.* **509**, 181–206.

Ross, A. N., Linden, P. F. & Dalziel, S. B. 2002 A study of three-dimensional gravity currents on a uniform slope. *J. Fluid Mech.* **453**, 239–261.

Shin, J. O., Dalziel, S. B. & Linden, P. F. 2004 Gravity currents produced by lock exchange. *J. Fluid Mech.* **521**, 1–34.

Simpson, J. E. 1997 Gravity currents in the environment and the laboratory. 2nd edn. Cambridge University Press.

Tickle, G. A. 1996 A model of the motion and dilution of a heavy gas cloud released on a uniform slope in calm conditions. *J. Haz. Mat.* **49**, 29–47.

Tochon-Danguey, J. C. 1977 Étude des courant de gravité sur fort pente avec application aux avalanches poudreuse. These, *L'Universite Scientifique et Medicale de Grenoble*.

Webber, D. M., Jones, S. J. & Martin, D. 1993 A model of the motion of a heavy gas cloud released on a uniform slope. *J. Haz. Mat.* **33**, 101–122.